Methods

miniTurbo-based interactomics of two plasma membrane-localized SNARE proteins in *Marchantia polymorpha*

Katharina Melkonian[1] (iD), Sara Christina Stolze[2] (iD), Anne Harzen[1,2] (iD) and Hirofumi Nakagami[1,2] (iD)

[1]Basic Immune System of Plants, Max-Planck Institute for Plant Breeding Research, Carl-von-Linné-Weg 10, 50829, Cologne, Germany; [2]Protein Mass Spectrometry, Max-Planck Institute

for Plant Breeding Research, Carl-von-Linné-Weg 10, 50829, Cologne, Germany

Author for correspondence:
Hirofumi Nakagami
Email: nakagami@mpipz.mpg.de

Summary

• *Marchantia polymorpha* is a model liverwort and its overall low genetic redundancy is advantageous for dissecting complex pathways. Proximity-dependent *in vivo* biotin-labelling methods have emerged as powerful interactomics tools in recent years. However, interactomics studies applying proximity labelling are currently limited to angiosperm species in plants.

• Here, we established and evaluated a miniTurbo-based interactomics method in *M. polymorpha* using MpSYP12A and MpSYP13B, two plasma membrane-localized SNARE proteins, as baits.

• We show that our method yields a manifold of potential interactors of MpSYP12A and MpSYP13B compared to a coimmunoprecipitation approach. Our method could capture specific candidates for each SNARE.

• We conclude that a miniTurbo-based method is a feasible tool for interactomics in *M. polymorpha* and potentially applicable to other model bryophytes. Our interactome dataset on MpSYP12A and MpSYP13B will be a useful resource to elucidate the evolution of SNARE functions.

Introduction

The liverwort *Marchantia polymorpha* is a well-established model plant. The *M. polymorpha* genome has been sequenced (Bowman *et al.*, 2017; Montgomery *et al.*, 2020) and genetic tools have been developed (Ishizaki *et al.*, 2008, 2013, 2015; Kubota *et al.*, 2013). In *M. polymorpha*, there is no evidence for whole genome duplication during evolution and the number of paralogues for many regulatory genes is rather low in comparison with other model plants (Bowman *et al.*, 2017). Accordingly, low genetic redundancy is a useful feature of *M. polymorpha* in dissecting the basic mechanisms and gene functions underlying complex pathways.

Elucidating complex pathways and protein-interaction networks remain major challenges in plant research. Conventional approaches to study protein–protein interactions, such as coimmunoprecipitation (Co-IP) followed by mass spectrometry (MS), have limitations. Successful enrichment and purification under nonphysiological conditions require a certain binding affinity between interactors. Therefore, Co-IP is often effective in capturing stable complexes, while weak and transient associations can easily be lost. The analysis of interactions between members of subcellular proteomes may require an enrichment of cellular compartments before Co-IP to avoid artificial interactions upon cell lysis. In this context, proximity-dependent *in vivo* labelling (PL) approaches are gaining an increasing importance as alternative interactomics approaches.

The miniTurbo-based PL method was initially established in bacterial and mammalian cells, and is based on biotin ligase-mediated labelling of interaction partners with exogenously applied biotin (Branon *et al.*, 2018). TurboID is a promiscuous biotin ligase that has been engineered from *Escherichia coli* BirA with 15 mutations and has a higher ligase activity at a wide range of temperatures compared to BirA. The miniTurbo is a smaller version of TurboID with a deleted N-terminal domain and has 13 mutations compared to BirA. TurboID and miniTurbo were reported to have higher activities than other biotin ligases, namely BioID, BioID2 and BASU, in HEK 293T cells. Compared to TurboID, miniTurbo was found to be overall 1.5 times less active and showed a lower background labelling activity without exogenous application of biotin in HEK 293T cells (Branon *et al.*, 2018). For PL of interaction partners, the biotin ligase is fused to a bait. Molecules in proximity of the bait are biotinylated by the ligase in the presence of biotin. After labelling, biotinylated proteins can be extracted and enriched by streptavidin-pulldown before identification by MS.

For pulldown of biotinylated proteins, it is not required that proteins and complexes remain in their native state, because enrichment of biotinylated proteins does not rely on affinity to the bait proteins. PL approaches can thus also capture weak or transient interactions. The binding affinity between biotin and streptavidin is high. Therefore, protein extraction, binding and washing steps can be conducted in the presence of high concentrations of detergents. The ligase activity can be inactivated during protein extraction, and thus artificial labelling upon cell lysis will not occur. This is advantageous for investigating interactions of proteins in subcellular compartments, including plasma membrane-localized proteins.

Since biotin ligases do not distinguish between real interaction partners and other molecules residing in proximity of the bait by chance, a certain level of unspecific labelling is expected. Unspecific labelling may occur according to expression of the bait in a specific cellular compartment, cell type, tissue, organ, at a specific developmental stage or physiological status and will be enhanced under saturating labelling conditions. Therefore, non-saturating labelling conditions are desirable and appropriate controls should be designed to narrow down candidates of high confidence by minimizing false positive identifications (Mair *et al.*, 2019).

Plants, unlike animals, can synthesize biotin *de novo* (Baldet *et al.*, 1993, 1997). High levels of endogenous biotin may lead to background labelling, potentially interfering with PL approaches. The endogenous biotin level in *M. polymorpha* has not been investigated. In *Arabidopsis thaliana*, the sucrose-H$^+$ symporter AtSUC5 was identified to mediate uptake of exogeneous biotin (Ludwig *et al.*, 2000; Pommerrenig *et al.*, 2013). To date, AtSUC5 remains the only sucrose transporter that has been shown to function in biotin uptake *in planta*. It is not yet known whether comparable mechanisms for biotin uptake exist in *M. polymorpha*.

The TurboID or miniTurbo method has been successfully applied in *A. thaliana*, *Nicotiana benthamiana* and *Solanum lycopersicum* using stable transgenic lines or transient expression systems, to efficiently label and identify subcellular proteomes in specific cell types (Mair *et al.*, 2019) as well as interacting partners of cytosolic (Zhang *et al.*, 2019; Arora *et al.*, 2020) and nuclear (Mair *et al.*, 2019) bait proteins by MS. Arora *et al.* (2020) demonstrated that TurboID can be applied to detect known interactions of plasma membrane-localized proteins with a targeted approach using immunoblotting. However, a direct comparison of interactomics applying Co-IP and PL using the same plant materials is still missing. It remains unclear whether biotin ligase-mediated PL approaches can be sensitive and specific to reveal differences in interactomes of very similar proteins, such as closely related homologus. Lastly, in bryophyte species, an interactome study utilizing PL approaches has not yet been reported.

In *M. polymorpha*, two SNARE (soluble *N*-ethylmaleimide-sensitive factor attachment protein receptor) proteins, MpSYP12A and MpSYP13B, are plasma membrane-localized and ubiquitously expressed throughout the thallus (Kanazawa *et al.*, 2016, 2020). Plant SNAREs modulate membrane-trafficking, intra- and intercellular signalling, and transport. In *A.*

thaliana, 65 SNARE proteins have been identified, nine of which are SYP1 family proteins that are plasma membrane-localized (Uemura *et al.*, 2004). During land plant evolution, the expansion of SNARE proteins and their functional diversification was hypothesized to be linked to multicellularity and probably facilitated adaptation to a terrestrial lifestyle (Sanderfoot, 2007). Thus, land plant secretory pathways are highly sophisticated, dynamic and diversely regulated, being involved in a manifold of cellular processes ranging from polarized growth to defence responses (Batoko & Moore, 2001; Collins *et al.*, 2003; Catalano *et al.*, 2007; Enami *et al.*, 2009; Silva *et al.*, 2010; Reichardt *et al.*, 2011; Uemura *et al.*, 2012; Ichikawa *et al.*, 2014; Johansson *et al.*, 2014; Yun *et al.*, 2016; Xia *et al.*, 2019; Hirano *et al.*, 2020; Rubiato *et al.*, 2021). In *M. polymorpha*, the SYP1 protein family consists of four members: SYP12A, SYP12B, SYP13A and SYP13B. MpSYP13A and MpSYP13B belong to the SYP13 group and are closely related to AtSYP131 and AtSYP132. MpSYP12A and MpSYP12B belong to the SYP11/12 group, which is phylogenetically separated from the SYP11 or SYP12 group proteins in angiosperms (Kanazawa *et al.*, 2016; Bowman *et al.*, 2017). Carella *et al.* (2018) reported that MpSYP13B accumulated in haustoria-like structures upon infection of *M. polymorpha* with the oomycete pathogen *Phytophthora palmivora*. Recently, MpSYP12A was shown to localize to the phragmoplast during cell plate formation (Kanazawa *et al.*, 2020). Interaction partners of SYP1 family proteins in *M. polymorpha* have not yet been identified.

In this study, we have established a miniTurbo-based PL method for interactome profiling in *M. polymorpha*. Using MpSYP12A and MpSYP13B as baits, we evaluated biotin labelling conditions and a procedure to enrich biotinylated proteins, and then potential interactors were identified by MS. We directly compared the performances of Co-IP and PL approaches using the same plant materials. Lastly, by comparing the identified interactomes of MpSYP12A and MpSYP13B, we found potential interactors that are specific to each SNARE.

Materials and Methods

Construction and cloning

Gateway entry vectors containing genomic sequences for an expression of *M. polymorpha* MpSYP12A and MpSYP13B under their own regulatory elements (5′- and 3′-flanking sequences and introns) in *M. polymorpha* were provided by T. Ueda (Kanazawa *et al.*, 2016). For N-terminal tagging of MpSYP12A and MpSYP13B with miniTurbo and Myc-tag, entry vector backbones were linearized by restriction with *Sma*I or *Bam*HI enzymes, respectively. Codon-optimized miniTurbo (Supporting Information Fig. S1) was synthesized by Thermo GeneArt and amplified from a donor plasmid by PCR. Gateway entry vectors pMKMM20 (3.5 kb upstream of *SYP13B:5′UTR:miniTurbo-Myc-SYP13B:3′UTR*) and pMKMM21 (3.5 kb upstream of *SYP12A:5′UTR:miniTurbo-Myc-SYP12A:3′UTR*) were generated by in-fusion cloning (HD enzyme mix; Takara Bio, Shiga, Japan). Gateway binary vectors pMKMM22 and pMKMM23

for the expression of miniTurbo-Myc-MpSYP13B and miniTurbo-Myc-MpSYP12A were generated by LR-recombination (LR clonase; Invitrogen) of pMKMM20 or pMKMM21 with pMpGWB301 (Fig. S2).

Marchantia polymorpha lines used in this study

The male *M. polymorpha* Takaragaike-1 (Tak-1) ecotype was used as a wild-type. Transgenic lines in the Tak-1 background were generated using the cut thallus method (Kubota *et al.*, 2013) and *Agrobacterium* strain GV3101 carrying pMKMM22 or pMKMM23. Transformants were selected using chlorsulfuron and cefotaxime antibiotics for two generations. Selected transformants were screened for expression of miniTurbo-Myc-MpSYP12A and miniTurbo-Myc-MpSYP13B fusion proteins by immunoblotting. Transgenic lines were chosen that displayed similar expression levels of miniTurbo-Myc-MpSYP12A and miniTurbo-Myc-MpSYP13B for further analyses (Figs S3a, S6). *Marchantia polymorpha* plants were grown and maintained on Gamborg's B5 (G0209; Duchefa, Haarlem, the Netherlands) half-strength solid medium containing 1% plant agar in a walk-in growth chamber under 50–60 µmol photons $m^{-2} s^{-1}$ continuous white light-emitting diode (LED) light at 22–24°C.

Sample preparation for PL and Co-IP experiments

Marchantia polymorpha Tak-1 and transgenic lines were grown from single gemmae on Gamborg's B5 half-strength solid medium containing 0.8% plant agar for 10 d under 50–60 µmol photons $m^{-2} s^{-1}$ continuous white LED light at 22–24°C. Ten individual 10-d-old thalli were pooled per sample. For Co-IP, untreated thalli were sampled immediately and frozen in liquid nitrogen until further processing. For biotin treatment, thalli were transferred into transparent six- or 12-well plates (657160; Greiner Bio-One, Stonehouse, UK) and submerged in 0–700 µM biotin (B4501; Sigma) solution in water. The thalli were vacuum-infiltrated with biotin solutions for 5 min using a desiccator and the samples were incubated for 0–24 h at room temperature (RT; 22–25°C) while shaking. After incubation, the thalli were washed once with ice-cold ultrapure water for 2 min to remove excess biotin. For sampling, thalli were transferred onto filter paper (1001-085; Whatman) and left for 10 s to drain off excess liquid. Next, the thalli were pressed onto the filter paper for 5 s, immediately transferred to fresh tubes containing two stainless-steel beads and snap-frozen in liquid nitrogen. The plant material was ground in liquid nitrogen using a mixing mill (MM400; Retsch) for 5 min at 30 Hz. For Co-IP, all the following steps were conducted at 4°C. The finely ground powder was mixed with extraction buffer (50 mM Tris–HCl pH 7.5, 150 mM NaCl, 10% glycerol, 2 mM ethylenediaminetetraacetic acid (EDTA), 5 mM dithiothreitol (DTT), 1% Triton X-100, 1% Protease Inhibitor Cocktail (P9599; Sigma)) and incubated for 30 min for protein extraction. For PL samples, the powder was mixed with 500 µl preheated SDT buffer (100 mM Tris–HCl pH 7.5, 4% sodium dodecyl sulphate (SDS), 0.1 M DTT)
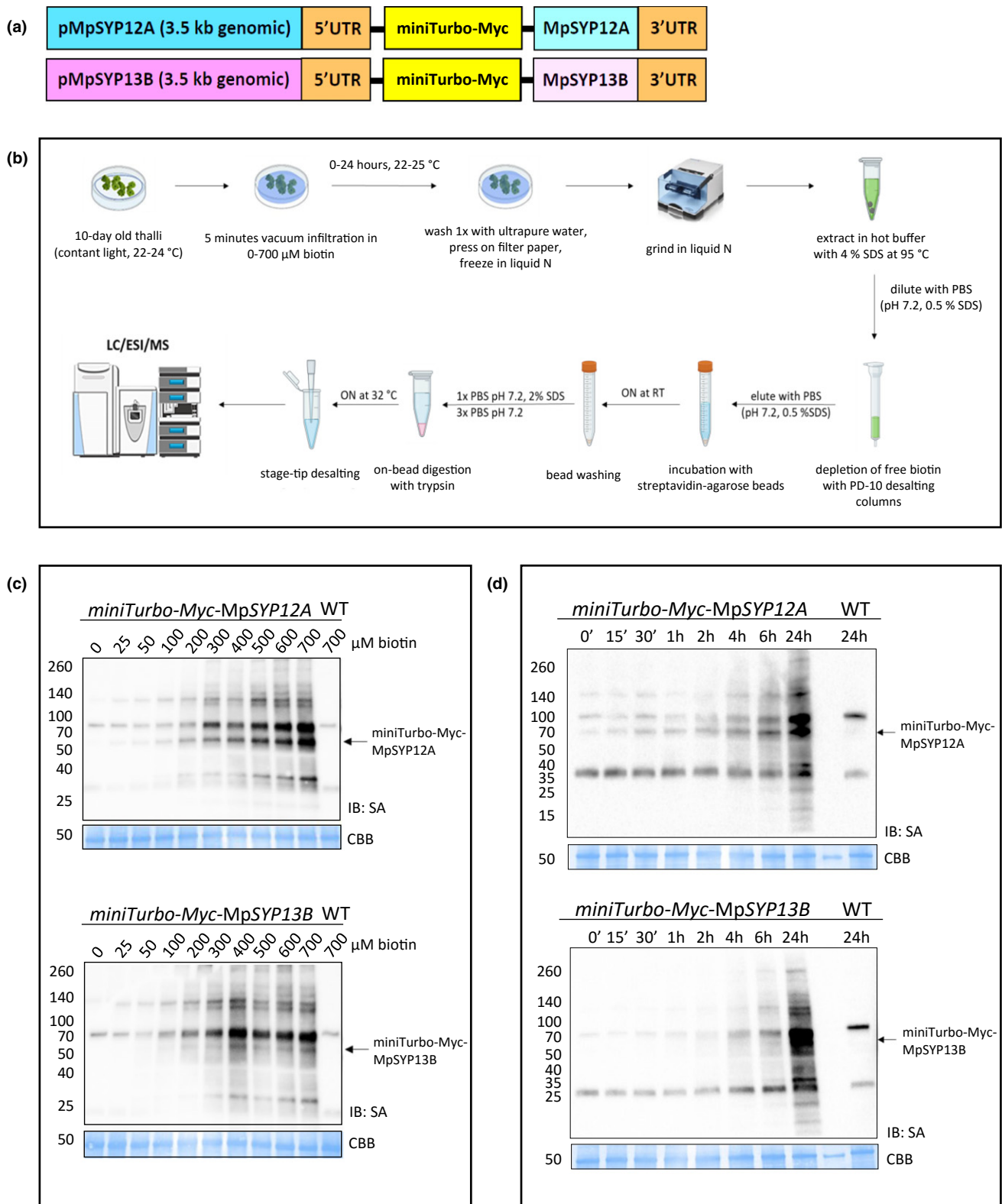
at 95°C for 5 min and then sonicated for 10 min. Cell debris was removed from the extracts by two consecutive centrifugation steps (10 000 g, 10 min). The protein concentration in cell extracts for Co-IP and PL was determined using the Pierce 660 nm Assay (22660; Thermo Fisher, Waltham, MA, USA). Cell extracts with 500 µg of total protein were used as input for Myc-Trap Co-IP and biotin depletion before affinity-pulldown of biotinylated proteins. For biotin-treated thalli, an aliquot of each sample was taken for immunoblotting and whole proteome analysis. The remaining samples were subjected to biotin depletion before pulldown using streptavidin. Biotin dilution series and time course experiments were each done in two independent experiments (Figs 1c,d, S4a,b, S6).

Co-IP

Myc-Trap beads (ytma-20; Chromotek, Planegg, Germany) were equilibrated in ice-cold wash buffer (50 mM Tris–HCl pH 7.5, 150 mM NaCl, 10% glycerol, 2 mM EDTA) according to the manufacturer's instructions. Cell extracts with 500 µg of total protein in 1 ml volume were mixed with 25 µl of equilibrated Myc-Trap beads and pulldown was performed for 2 h at 4°C on a rolling wheel. Myc-Trap beads were magnetically separated from the supernatant and washed three times in 500 µl wash buffer. An aliquot corresponding to 10% of the beads was used for immunoblotting and the remaining beads were subjected to on-bead digestion with trypsin. For immunoblotting of Co-IP samples, the proteins were eluted from the beads in 30 µl 4× SDS sample buffer (250 mM Tris–HCl pH 6.8, 40% glycerol, 8% SDS, 0.08% bromophenol blue, 200 mM DTT) by boiling for 10 min at 95°C.

Depletion of free biotin

Biotin depletion methods were tested using a transgenic line expressing miniTurbo-Myc-MpSYP13B and Tak-1. Cell extracts were prepared as described above from 10-d-old thalli treated with 700 µM biotin for 24 h. As input, 500 µg of total protein in 500 µl SDT buffer was used per sample. For methanol : chloroform precipitation, 666 µl methanol and 166 µl chloroform were added to the cell extracts and the samples were mixed. Next, 300 µl water was further added and mixed, and then centrifuged for 10 min at 1500 g. The separated upper and lower liquid phases were removed. The solid white layer containing precipitated proteins that had formed between the liquid phases was kept. The protein pellet was resuspended in 600 µl methanol and sonicated for 10 min. After centrifugation for 10 min at 16 100 g, the supernatant was removed completely. The protein pellets were air-dried for 5 min and resuspended in 500 µl SDT buffer. After 10 min of sonication, the samples were incubated for 30 min at RT while shaking at 1000 rpm, until the protein pellets were redissolved. The samples were then diluted with phosphate-buffered saline (PBS buffer: 0.1 M phosphate, 0.15 M NaCl, pH 7.2) to a final concentration of 0.5% SDS. For biotin depletion with PD-10 desalting columns (17085101; VWR), the columns were equilibrated with SDT : water (1 : 5) and the cell extracts

(a)

| pMpSYP12A (3.5 kb genomic) | 5'UTR | miniTurbo-Myc | MpSYP12A | 3'UTR |

| pMpSYP13B (3.5 kb genomic) | 5'UTR | miniTurbo-Myc | MpSYP13B | 3'UTR |

(b)

(c)

(d)

Fig. 1 Experimental setup for miniTurbo-mediated biotin labelling in *Marchantia polymorpha*. (a) Schematic representation of the constructs used for generating transgenic plants. (b) Overview of the workflow used for evaluating the miniTurbo-based interactomics method in *M. polymorpha*. The figure was created with elements from BioRender (https://biorender.com). (c, d) Biotin ligase activity in *M. polymorpha*. Streptavidin (SA) immunoblots (IB) of cell extracts from *M. polymorpha* transgenic lines expressing miniTurbo-Myc-MpSYP12A (upper panels) and miniTurbo-Myc-MpSYP13B (lower panels) that were (c) treated with 0–700 µM biotin solutions for 24 h at room temperature (RT) or (d) treated with 700 µM biotin solution for 0–24 h at RT. Cell extracts of wild-type Tak-1 (WT) treated with 700 µM biotin solution for 24 h were used as a control. Arrows indicate the positions of the biotinylated miniTurbo-Myc-MpSYP12A and miniTurbo-Myc-MpSYP13B fusion-proteins. Coomassie Brilliant Blue-stained (CBB) membranes are shown as loading controls.

were diluted to 2.5 ml with ultrapure water. PD-10 desalting was performed according to the manufacturer's instructions and the proteins were eluted with 3.5 ml PBS buffer containing 0.5% SDS. For biotin depletion using Zeba spin columns (89893; Thermo Fisher), the columns were equilibrated with SDT : water (1 : 5) and the cell extracts were diluted to 2.5 ml with ultrapure water. Desalting was then performed according to the manufacturer's instructions. All biotin-depleted samples were adjusted to 4 ml final volume with binding buffer (0.1 M phosphate, 0.15 M NaCl, 0.5% SDS, pH 7.2) before pulldown. Aliquots of intermediate steps were taken for immunoblotting. All biotin depletion methods were tested at the same time in duplicates. PD-10 column desalting was used for the pulled-down samples measured by MS.

Pulldown of biotinylated proteins

Biotinylated proteins were pulled-down using streptavidin-agarose beads (20353; Thermo Fisher). Per sample, 100 µl of a 50% slurry was used. The beads were washed and equilibrated in the binding buffer. Next, the biotin-depleted samples were added to the beads and pulldown was performed overnight at RT while mixing. The beads were washed once with 6 ml PBS buffer containing 2% SDS and then three times with 10 ml PBS buffer. Aliquots of all samples were taken during intermediate steps and an aliquot corresponding to 10% of the washed beads was taken after pulldown for immunoblotting. The proteins were eluted from the beads by boiling for 10 min at 95°C in 50 µl 4× SDS sample buffer containing 20 mM biotin while shaking at 1000 rpm. For immunoblots, 20% of the IP-eluate was used, corresponding to 2% of the input amount of beads. The remaining beads from pulldown with bound biotinylated proteins were subjected to on-bead digestion for MS analysis.

On-bead digestion

For Myc-IP and streptavidin-pulldown samples, Myc-Trap beads or streptavidin-agarose beads were resuspended in 25 µl digest buffer 1 (50 mM Tris–HCl pH 7.5, 2 M urea, 1 mM DTT, 5 µg µl^{-1} trypsin) and incubated at 30°C for 30 min while shaking at 400 rpm. The supernatant was separated from the beads magnetically or by sedimentation and transferred to a fresh tube. The beads were then mixed with 50 µl digest buffer 2 (50 mM Tris–HCl pH 7.5, 2 M urea, 5 mM chloroacetamide (CAA)), and the supernatant was separated from the beads and combined with the supernatant from the previous step. The combined supernatant was further incubated overnight at 32°C while shaking at 400 rpm. Trypsin was inactivated by acidification with tri-fluoroacetic acid (TFA), and the peptide sample was subsequently desalted using C$_{18}$ stage tips (Rappsilber *et al.*, 2003).

Sample preparation for whole proteome analyses

Aliquots of cell extracts from biotin labelling experiments were used for whole proteome analysis. The extracts were processed using a filter-aided sample preparation (FASP) protocol adapted from Wisniewski *et al.* (2009). In brief, 50 µg of total protein extract was used as input. The proteins were alkylated using CAA and digested using LysC and trypsin. The peptide solutions were desalted using C$_{18}$ stage tips. Whole proteome analyses were conducted for one representative replicate per genotype and condition.

LC-MS/MS data acquisition

The dried peptides from filter-aided digestion were redissolved in buffer A (2% acetonitrile (ACN), 0.1% TFA) and adjusted to a final peptide concentration of 0.1 µg µl^{-1} for analysis. The peptide samples from streptavidin- and Myc-Trap pulldowns were dissolved in 10 µl buffer A and measured without dilution.

PL samples were analysed using an EASY-nLC 1200 (Thermo Fisher) coupled to a Q Exactive Plus mass spectrometer (Thermo Fisher). The peptides were separated on 16 cm frit-less silica emitters (75 µm inner diameter; New Objective, Littleton, MA, USA), packed in-house with reversed-phase ReproSil-Pur C18 AQ 1.9 µm resin (Dr. Maisch). The peptides were loaded on the column and eluted for 50 min using a segmented linear gradient of 5% to 95% solvent B (0 min: 5% B; 0–5 min → 5% B; 5–25 min → 20% B; 25–35 min → 35% B; 35–40 min → 95% B; 40–50 min → 95% B) (solvent A: 0% ACN, 0.1% formic acid (FA); solvent B: 80% ACN, 0.1% FA) at a flow rate of 300 nl min^{-1}. Mass spectra were acquired in data-dependent acquisition mode with a TOP10 method. MS spectra were acquired in the Orbitrap analyser with a mass range of 300–1500 *m/z* at a resolution of 70 000 FWHM (full width at half maximum) and a target value of 3×10^6 ions. Precursors were selected with an isolation window of 1.3 *m/z*. HCD (higher energy collisional dissociation) fragmentation was performed at a normalized collision energy of 25. MS/MS spectra were acquired with a target value of 5×10^5 ions at a resolution of 17 500 FWHM, a maximum injection time of 85 ms and a fixed first mass of *m/z* 100. Peptides with a charge of 1, >6 or with unassigned charge state were excluded from fragmentation for MS^2; dynamic exclusion for 20 s prevented repeated selection of precursors.

Myc-IP and whole proteome samples were analysed using an EASY-nLC 1000 coupled to a Q Exactive mass spectrometer (both Thermo Fisher). The peptides were separated on 16 cm frit-less silica emitters (75 µm inner diameter; New Objective), packed in-house with reversed-phase ReproSil-Pur C18 AQ 1.9 µm resin (Dr. Maisch). Peptides (0.5 µg) were loaded on the column and eluted for 115 min using a segmented linear gradient of 5% to 95% solvent B (0 min: 5% B; 0–5 min → 5% B; 5–65 min → 20% B; 65–90 min → 35% B; 90–100 min → 55% B; 100–105 min → 95% B; 105–115 min → 95% B) at a flow rate of 300 nl min^{-1}. Mass spectra were acquired in data-dependent acquisition mode with a TOP15 method. MS spectra were acquired in the Orbitrap analyser with a mass range of 300–1750 *m/z* at a resolution of 70 000 FWHM and a target value of 3×10^6 ions. Precursors were selected with an isolation window of 2.0 *m/z*. HCD fragmentation was performed at a

normalized collision energy of 25. MS/MS spectra were acquired with a target value of 10^5 ions at a resolution of 17 500 FWHM, a maximum injection time of 55 ms and a fixed first mass of m/z 100. Peptides with a charge of 1, > 6 or with unassigned charge state were excluded from fragmentation for MS^2; dynamic exclusion for 30 s prevented repeated selection of precursors.

Data analysis

Raw data were processed using Max Quant software (v.1.6.3.4, http://www.maxquant.org/) (Cox & Mann, 2008) with label-free quantification (LFQ) and intensity-based absolute quantification (iBAQ) enabled (Tyanova *et al.*, 2016). For PL data, normalization was skipped for the LFQ quantification. MS/MS spectra were searched by the Andromeda search engine against a combined database containing the sequences from *M. polymorpha* (MpTak1v5.1_r1_primary_transcripts_proteinV2; http://marchantia.info/ (Montgomery *et al.*, 2020)) and sequences of 248 common contaminant proteins and decoy sequences and the sequence of miniTurbo. Trypsin specificity was required with a maximum of two missed cleavages allowed. Minimal peptide length was set to seven amino acids. Carbamidomethylation of cysteine residues was set as fixed, and oxidation of methionine and protein N-terminal acetylation were set as variable modifications. Peptide-spectrum matches and proteins were retained if below a false discovery rate (FDR) of 1%. For PL data, the nonnormalized MaxLFQ values of all replicates (four per condition) were preprocessed in Perseus (v.1.5.8.5) and submitted for normalization analysis using the Normalyzer tool (http://normalyzer.immunoprot.lth.se/ (Chawade *et al.*, 2014)). The output was analysed for outliers and one replicate per condition was removed. The final data analysis was conducted in MaxQuant as described above on the reduced raw dataset. Statistical analysis of the MaxLFQ values was conducted using Perseus (v.1.5.8.5, http://www.maxquant.org/). Quantified proteins were filtered for reverse hits and hits 'identified by site' and MaxLFQ values were log$_2$ transformed. For PL data, transformed MaxLFQ values were normalized by subtraction of the median per column. After grouping samples by condition, only those proteins that had three or two valid values in one of the conditions for PL data or Myc-IP data, respectively, were retained for subsequent analysis. Two-sample *t*-tests were performed using a permutation-based FDR of 5%. For the generation of volcano plots, missing values were imputed from a normal distribution using the default settings in Perseus (1.8 downshift, separately for each column) for data with three valid values in one of the conditions. Volcano plots were generated in Perseus using an FDR of 5% and an $S0 = 1$. The Perseus output was exported and further processed using Microsoft Excel and RStudio (v.1.4.1103, https://www.rstudio.com/) based on R (v.x64 4.0.3, https://cran.r-project.org/). The data were processed in RStudio using the tidyverse (v.1.3.0), rio (v.0.5.16) and zoo (v.1.8-8) packages. Relative iBAQ values were calculated per column from MaxQuant output, scaled by a factor of 10^6 and log$_{10}$ transformed. The median value of three replicates

per condition was used to generate volcano plots including relative iBAQ values. Volcano plots were generated in RStudio using the ggplot 2 (v.3.3.3), ggrepel (v.0.9.1) and ggsci (v.2.9) packages.

Immunoblotting

Proteins were separated by SDS-polyacrylamide-gel electrophoresis (PAGE) and blotted onto polyvinylidene fluoride (PVDF) membranes (1704272; Bio-Rad) using a Trans-Blot Turbo (Bio-Rad) transfer system. The following antibodies were used: horseradish peroxidase (HRP)-conjugated streptavidin (streptavidin-HRP: 3999S; Cell Signaling, Danvers, MA, USA), anti-Myc-tag mouse monoclonal antibody (9B11; Cell Signaling) and HRP-conjugated antimouse immunoglobulin G (IgG) antibody (7076S; Cell Signaling). The membranes were probed for biotinylated proteins with streptavidin-HRP for 45 min to 3 h at RT. For detection of miniTurbo-Myc, the membranes were probed with anti-Myc-tag primary antibody overnight at 4°C and then with antimouse IgG secondary antibody for 1 h at RT. Biotinylated proteins or Myc-tagged miniTurbo were visualized on the membranes using a luminol-based chemiluminescent substrate that is oxidized by HRP in the presence of peroxide (34577; Thermo Fisher). The membranes were then stained with Coomassie staining solution (60 mg l^{-1} Coomassie brilliant blue, 10% acetic acid).

Annotations and gene ontology (GO) analyses

For *M. polymorpha* protein annotation, gene annotations from MpTak1_v5.1 and JGI 3.1 (https://marchantia.info/) were integrated. Information of *A. thaliana* homologues was further used for the annotation. A Basic Local Alignment Search Tool (Blast) was used to determine homologues in *A. thaliana* (TAIR10). The best hit with an *e*-value $\leq 10^{-10}$ was defined as a homologue. TAIR10 (https://www.arabidopsis.org/ (Lamesch *et al.*, 2012)), Panther v.16.0 (http://pantherdb.org/ (Mi *et al.*, 2021)), String 11.5 (https://string-db.org/ (von Mering *et al.*, 2003)), BioGrid 4.4 (https://thebiogrid.org/ (Stark *et al.*, 2006)) and IntAct 1.0.2 (https://www.ebi.ac.uk/intact/home (Orchard *et al.*, 2014)) were used for annotating *A. thaliana* homologues (Dataset S1). RStudio (v.1.4.1103, https://www.rstudio.com/), based on R (v.x64 4.0.3, https://cran.r-project.org/), the tidyverse (v.1.3.0), rio (v.0.5.16) and zoo (v.1.8-8) packages, were used for integrating annotation files. GO-term enrichment analysis was performed with Metascape 3.5 (https://metascape.org/ (Zhou *et al.*, 2019)) using express analysis settings. Corresponding *A. thaliana* homologues were used as input protein lists for the analysis. A list of reported and predicted interactors of AtSYP1 proteins was generated by integrating information from the BioGrid, IntAct and STRING databases (Dataset S2). Blast was used to determine homologues in *M. polymorpha* (JGI 3.1). The best hit with an *e*-value $\leq 10^{-10}$ was defined as a homologue (Dataset S3). Panther v.16.0 and PPDB (http://ppdb.tc.cornell.edu/ (Sun *et al.*, 2009)) were used to predict plasma membrane localization of *M. polymorpha* homologues.

Results

Experimental design for interactomics using miniTurbo-mediated PL and Co-IP in *M. polymorpha*

To potentially enhance transcription and translation efficiency of the bait-ligase fusion proteins in *M. polymorpha*, we used a codon-optimized version of the original miniTurbo (Fig. S1). We added a single Myc-tag to the C-terminus of miniTurbo, enabling not only the detection of the miniTurbo fusion proteins by immunoblotting, but also Co-IP experiments (Figs 1a, S1). We designed binary vectors to express miniTurbo-Myc-MpSYP12A and miniTurbo-Myc-MpSYP13B fusion proteins under the native promoters of Mp*SYP12A* and Mp*SYP13B* genes, respectively (Figs 1a, S2). The N-termini of these two MpSYPs are cytosolic, and N-terminal tagging of these SYPs with fluorescent proteins, which have similar size as miniTurbo, was demonstrated to be functional in *M. polymorpha* (Kanazawa *et al.*, 2016, 2020). Using these constructs, we generated stable transgenic lines in the wild-type Tak-1 background. Expression of the miniTurbo-Myc fusion proteins in candidate transformant lines was confirmed by immunoblotting using an anti-Myc antibody. To establish and evaluate the miniTurbo-based interactomics method, we selected transgenic lines showing similar expression levels for miniTurbo-Myc-MpSYP12A and miniTurbo-Myc-MpSYP13B. For this study, we used line No. 1 and line No. 3 for miniTurbo-Myc-MpSYP12A and miniTurbo-Myc-MpSYP13B, respectively (Figs S3a, S6).

In *A. thaliana*, Mair *et al.* (2019) demonstrated that levels of miniTurbo-mediated biotinylation of cellular proteins saturated when plants were treated with 50 µM biotin solution. Since uptake of exogenous biotin and levels of endogenously produced biotin are unknown in *M. polymorpha*, we treated the selected transgenic lines and Tak-1 with different concentrations of biotin, 0–700 µM, to find suitable conditions for *in vivo* biotin labelling. For biotin treatment, thalli were grown from single gemmae for 10 d, and then whole plants were submerged in biotin solutions and vacuum infiltrated for 5 min. We incubated the thalli in biotin solutions at 22–25°C for 24 h, a time point at which we expected a saturation of biotin labelling based on previous studies using miniTurbo in other plant species (Mair *et al.*, 2019; Zhang *et al.*, 2019). We subsequently checked the levels of biotinylated proteins in cell extracts by immunoblotting using streptavidin-HRP (Figs 1c, S4a, S6). We found increasing levels of biotinylated proteins with increasing biotin concentration in cell extracts of transgenic lines expressing either miniTurbo-Myc-MpSYP12A or miniTurbo-Myc-MpSYP13B but not in Tak-1. This confirmed biotin uptake and miniTurbo biotin ligase activity in *M. polymorpha* under the tested conditions. Given that levels of biotinylated proteins did not saturate for biotin concentrations up to 700 µM in *M. polymorpha*, we used 700 µM biotin solution in all following experiments. To determine suitable biotin treatment times in *M. polymorpha*, we next performed a time-course experiment and checked the levels of biotinylated proteins by immunoblotting after 0–24 h of biotin treatment (Figs 1d, S6). We detected increased levels of biotinylated

proteins in samples of transgenic lines expressing either miniTurbo-Myc-MpSYP12A or miniTurbo-Myc-MpSYP13B after 30 min of treatment (Figs S4b, S6), which further increased over time up to 24 h of treatment (Figs 1d, S6).

Previously published studies using TurboID and miniTurbo identified the depletion of free biotin after labelling as a critical step for pulldown of biotinylated proteins using streptavidin beads (Mair *et al.*, 2019; Zhang *et al.*, 2019, 2021; Arora *et al.*, 2020). We therefore tested three different approaches, methanol : chloroform precipitation, PD-10 gravity column desalting and Zeba spin column desalting, to remove excess free biotin from *M. polymorpha* cell extracts (Mair *et al.*, 2019; Saito *et al.*, 2019; Zhang *et al.*, 2019). Among these three methods, the methanol : chloroform precipitation approach has not been tested for free biotin depletion from plant materials. We used the miniTurbo-Myc-MpSYP13B line, which was treated with 700 µM biotin for 24 h. We evaluated biotin depletion based on pulldown efficiency, through immunoblotting of biotinylated proteins that could be eluted from the streptavidin-agarose beads after pulldown, and of nonbound biotinylated proteins that remained in the supernatant of the beads (Figs S3b,c, S6). Despite the fact that *M. polymorpha* thalli were treated with a higher concentration of biotin solution compared to other plant species, we found that all three methods could be used before affinity-pulldown to sufficiently enrich biotinylated proteins from *M. polymorpha* samples (Figs S3b, S6). With respect to easier handling, we used PD-10 column desalting for subsequent experiments.

The miniTurbo-based approach identifies a manifold of potential interactors of MpSYP12A and MpSYP13B in comparison to the Co-IP approach

A direct comparison between the performances of PL and Co-IP approaches for interactomics using the same plant materials has not yet been reported. We therefore performed IP of miniTurbo-Myc-MpSYP12A or miniTurbo-Myc-MpSYP13B using Myc-Trap beads from the same selected transgenic lines. After IP, we checked successful pulldown of the miniTurbo-Myc fusion proteins by immunoblotting. We detected miniTurbo-Myc-MpSYP12A and miniTurbo-Myc-MpSYP13B fusion proteins in the cell extract that was used as input for IP, and in IP eluates of samples from the transgenic lines (Figs S3d, S6). We then identified and quantified the proteins captured by Myc-IP using MS. Wild-type Tak-1 was used as a control. Three biological replicates were used for the analyses. We found a significant enrichment of the two bait proteins (Fig. 2a), confirming the immunoblotting result. Using Co-IP, we identified four and one potential interactors of MpSYP12A and MpSYP13B, respectively (Fig. 2a).

For the PL approach, we treated plants with biotin for 4 and 24 h to identify and quantify proteins after pulldown by MS. Wild-type Tak-1 was used as a control. Three biological replicates were used for analyses. As in the Co-IP approach, we found a significant enrichment of both baits using the miniTurbo-based approach (Fig. 2b,c). Four hours of biotin treatment resulted in
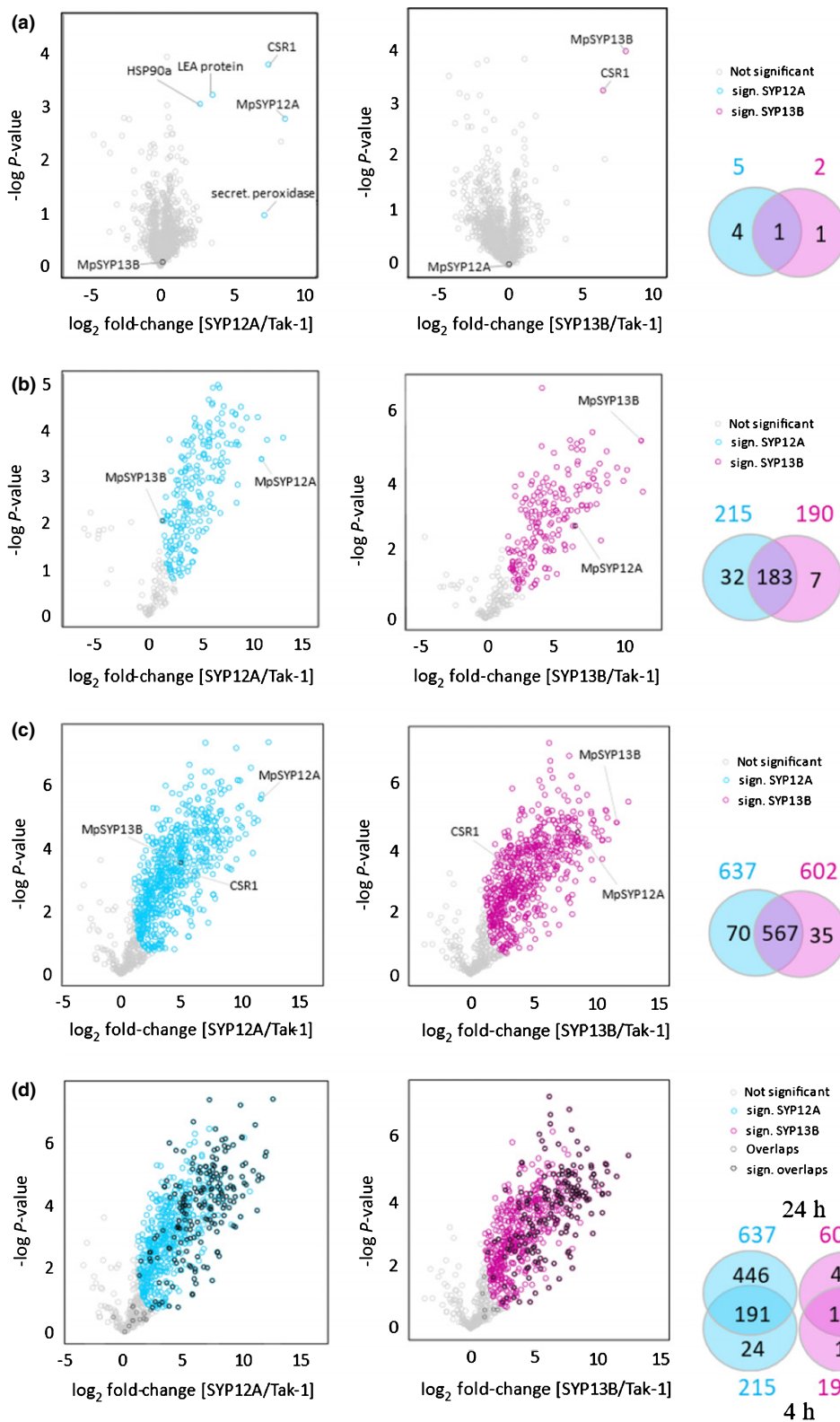
Fig. 2 Identification of MpSYP12A or MpSYP13B interacting proteins by coimmunoprecipitation (Co-IP) and proximity-dependent *in vivo* labelling (PL) approaches. *Marchantia polymorpha* wild-type Tak-1 was used as a control, and proteins that are significantly copurified with or biotinylated by the baits are highlighted. Three biological replicates were used for the analyses. Potential interacting proteins for MpSYP12A and MpSYP13B are shown in turquoise and magenta, respectively. Venn diagrams show numbers of the potential interactors and their overlap. (a) Myc-Trap Co-IP. Black text labels in volcano plots indicate the potential interactors for MpSYP12A or MpSYP13B. (b) 4 h PL. (c) 24 h PL. (d) Overlaps between 4 h and 24 h PL. Black circles in volcano plots indicate the potential interactors that are also identified with 4 h PL. Dark grey circles indicate proteins that are identified as the potential interactors with 4 h PL but not with 24 h PL.

an identification of 214 and 189 proteins as potential interactors of MpSYP12A and MpSYP13B, respectively (Fig. 2b). By increasing the treatment time to 24 h, the numbers of identified potential interactors nearly tripled (Fig. 2c). As expected, most of the candidates identified from 4 h samples were also identified from 24 h samples (Fig. 2d). In other words, approximately one-third of the candidates that were identified after 24 h of biotin treatment could be identified after 4 h of treatment. MpCSR1 (CHLORSULFURON RESISTANT 1), a potential interactor of MpSYP12A and MpSYP13B that we identified using Co-IP, was identified in the 24 h PL interactome dataset as well (Fig. 2c). Overall, these results demonstrate that PL approaches have a greater potential to identify undescribed interacting proteins compared to Co-IP approaches. However, note that the miniTurbo-based approach failed to identify proteins such as secretory peroxidases that are predicted to be secreted into the extracellular space (Fig. 2a). This is reasonable as miniTurbo was fused to the intracellular domain of MpSYPs. It is also of note that miniTurbo may interfere with Co-IP, and thus the use of small tags only, including the Myc-tag, may lead to different outcomes.

PL using MpSYP12A and MpSYP13B as baits enriches proteins involved in vesicle-mediated transport and plasma membrane-localized proteins

We next asked whether the potential interactors that we identified by PL overall fit with the expected biological function of MpSYP12A and MpSYP13B. For this, we annotated *M. polymorpha* proteins based on information of *A. thaliana* homologues (Dataset S1). We then performed GO term enrichment analysis of the 24 h interactome dataset using METASCAPE. Strikingly, 'vesicle-mediated transport' was the most significantly enriched GO term extracted from the interactome data for both MpSYP12A and MpSYP13B, coinciding with SNARE protein functions (Fig. 3a,b; Dataset S4). We also performed GO term enrichment analysis of proteome data that were obtained by measuring the input samples used for the streptavidin-pulldown. Enriched GO terms from proteome data were mainly related to primary metabolism (Fig. 3c), which is clearly distinct from the enriched GO terms of the interactome dataset (Fig. 3a,b). These results suggest that the potential interactors comprise actual interactors of MpSYP12A and MpSYP13B. Analysis of the 4 h interactome dataset gave similar results (Fig. S5a–c; Dataset S4).

A number of interactors of *A. thaliana* SNAREs, which are homologous to MpSYP12A and MpSYP13B, have been reported (Kwon *et al.*, 2008; Fujiwara *et al.*, 2014). Based on the BioGrid, STRING and IntAct databases, a total of 334 proteins were reported or predicted to interact with SYP1 proteins in *A. thaliana* (Dataset S2). Of these 334 *A. thaliana* proteins, we could identify 250 homologous proteins conserved in the *M. polymorpha* proteome using a BLAST approach (Dataset S3). Among these 250 proteins, we found that 47 and 40 were identified as potential interactors of MpSYP12A and MpSYP13B, respectively, while 39 were shared between both baits. Thus, the miniTurbo-based approach captured around 16–19% of

M. polymorpha proteins that are homologous to the reported *A. thaliana* SYP1 interacting proteins (Fig. 3d).

MpSYP12A and MpSYP13B were demonstrated to localize to the plasma membrane and to be ubiquitously expressed throughout the thallus in *M. polymorpha* (Kanazawa *et al.*, 2016). By using PANTHER GO annotations and *A. thaliana* plasma membrane proteome data, we predicted plasma membrane localizations of the potential interactors in *M. polymorpha* (Dataset S1). We found that more than one-third of the potential interactors are expected to be plasma membrane-localized (Fig. 3e). This result further supported the specificity and utility of the miniTurbo-based approach.

The miniTurbo-mediated approach can reveal subtle differences between very similar baits

By comparing the 24 h interactome data for MpSYP12A and MpSYP13B, we found that both baits share 90–95% of their potential interactors (Figs 1c, S6), which is reasonable considering their predicted functions. Still, we captured 52 and nine proteins that preferentially interact with MpSYP12A and MpSYP13B, respectively (Fig. 4a; Table 1). To investigate exclusive interaction partners of MpSYP12A and MpSYP13B, we implemented iBAQ values to the volcano plot (Fig. 4b). iBAQ is a measure of protein abundance, and relative abundance was reflected in different circle sizes. The respective colours indicate abundances in all pulldown samples. By this, we revealed that MpNEK1 (NIMA-related protein kinase 1) potentially interacts exclusively with MpSYP13B, and we found 13 proteins that potentially interact exclusively with MpSYP12A (Fig. 4b; Table 1).

Discussion

Published studies applying *in planta* TurboID-based PL have utilized model angiosperm species, and the amenability of current PL approaches to other plant species remains to be determined, as outlined by Mair & Bergmann (2021). Here, we successfully applied miniTurbo-based PL in the liverwort *M. polymorpha*. This confirmed the transferability of biotin ligase-utilized interactomics to a model bryophyte species.

We tested different biotin concentrations and treatment times to investigate biotin labelling of proteins in *M. polymorpha* cells. Mair *et al.* (2019) reported a saturation of biotinylated proteins in *A. thaliana* stable transgenic lines after treatment with 50 μM biotin solution for 1 h. Zhang *et al.* (2019) transiently expressed TurboID-fusion proteins in *N. benthamiana* leaves and tested biotin concentrations up to 800 μM. Zhang *et al.* observed that protein biotinylation was saturated after 8 h of treatment with 200 μM biotin, and that 15 min was sufficient for saturation at 200 μM biotin concentration. Meanwhile, in *M. polymorpha*, we did not observe a saturation of protein biotinylation after 24 h of treatment with 700 μM biotin. The observed differences in saturation of biotinylated proteins among the different studies could be partially explained by differences in mechanisms and efficiencies for biotin uptake and metabolism. Other factors potentially
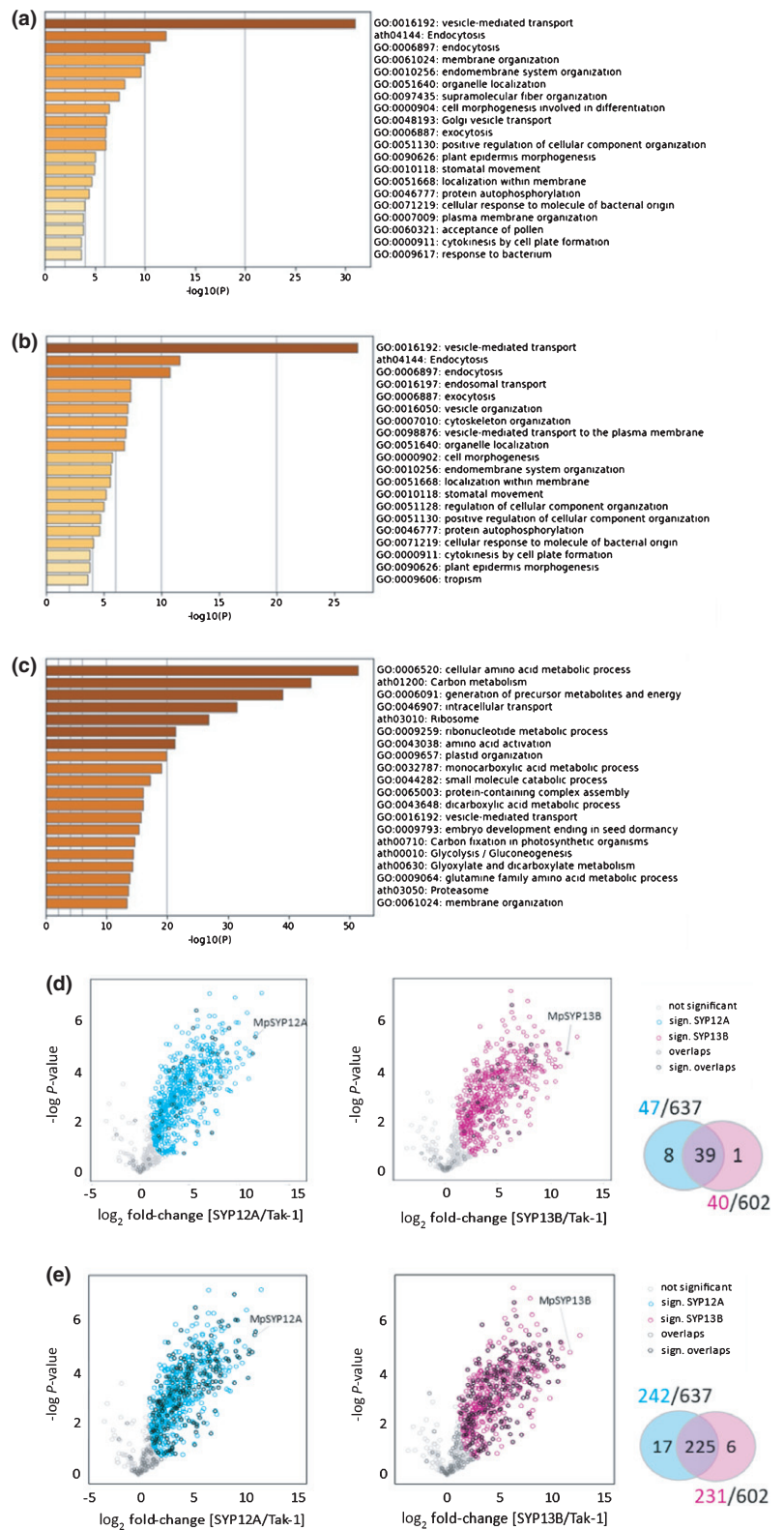
Fig. 3 Features of the identified MpSYP12A or MpSYP13B interacting proteins. (a–c) Gene ontology (GO) term enrichment analysis of (a) 24 h proximity-dependent *in vivo* labelling (PL) MpSYP12A interactome, (b) 24 h PL MpSYP13B interactome and (c) measured whole proteome. The top 20 overrepresented GO terms are shown. (d) *Marchantia polymorpha* homologues of AtSYP1-interacting proteins are highlighted in black or grey on volcano plots of 24 h PL. Venn diagram shows numbers of potential interactors that are homologous to the AtSYP1-interactors and their overlap. (e) Potential interactors that are predicted to localize to the plasma membrane are highlighted in black or grey on volcano plots of 24 h PL. Venn diagram shows numbers of the predicted plasma membrane-localized proteins and their overlap.

impacting biotin labelling activities are plant growth conditions such as light cycle and temperature used during biotin treatment.

For PL approaches, a careful evaluation of false positive candidates based on well-designed controls is desirable to generate a set of

candidates with high confidence for further analyses and validation. It would be beneficial to include other plasma membrane-localized proteins that are independent of MpSYP12A and MpSYP13B to aid in predicting false positive candidates, which might have been
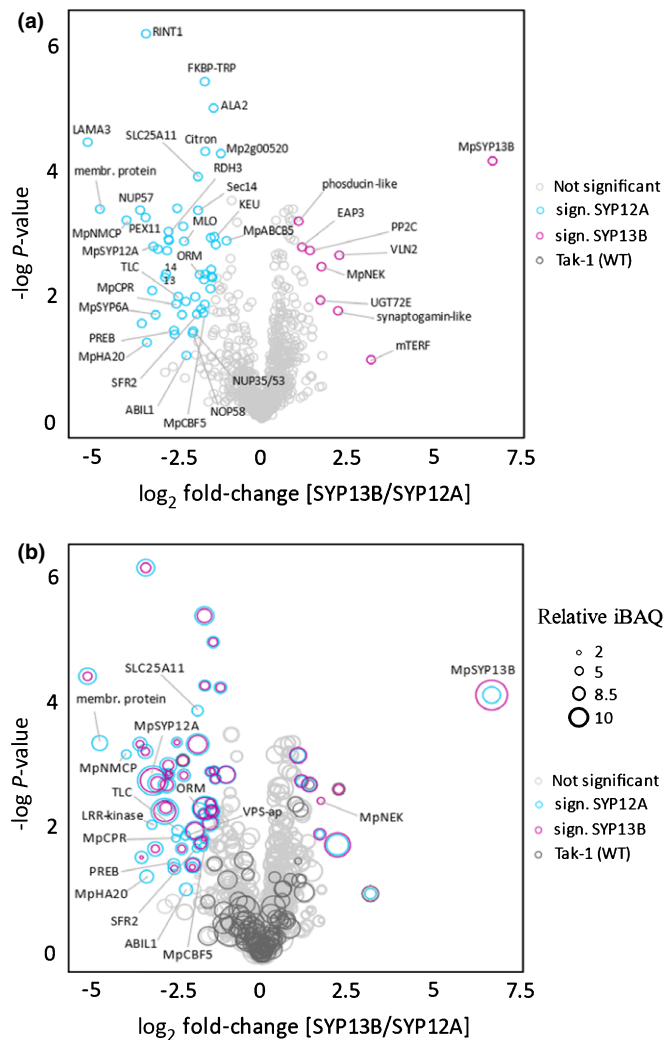
Fig. 4 Potential interactors that preferentially interact with MpSYP12A or MpSYP13B. (a) Proteins that preferentially interacted with MpSYP12A or MpSYP13B are highlighted in turquoise and magenta, respectively. (b) Relative protein abundances based on iBAQ values are indicated by sizes of circles. Protein abundances in the pulled-down samples of MpSYP12A, MpSYP13B and wild-type Tak-1 are shown in turquoise, magenta and dark grey, respectively. Proteins that were exclusively identified from the samples of MpSYP12A or MpSYP13B but not from the wild-type Tak-1 sample are annotated except for MpSYP12A and MpSYP13B. Three biological replicates were used for analyses.

biotinylated randomly due to their localizations. That is, our transgenic lines expressing miniTurbo-Myc-MpSYP12A and miniTurbo-Myc-MpSYP13B could be used as suitable controls for interactome mapping using other plasma membrane-localized baits in the future. Meanwhile, the overall high similarity between MpSYP12A and MpSYP13B can be exploited to investigate specific interactors to understand functional differences between the two SNAREs. In general, long biotin treatment times potentially increase false positive labelling. On the other hand, longer treatment times may be required to efficiently capture rare or transient interactors.

For biotin-labelling approaches, protein extraction can be conducted in the presence of strong detergents. Strong detergents facilitate the extraction and solubilization of membrane-

associated proteins, which can be advantageous for interactomics of plasma membrane-localized or organellar proteins. Our results confirmed that we could indeed capture a manifold of proteins that are predicted to be plasma membrane-localized, which has not been tested on the proteome level in published studies using PL in plants. In contrast to the Co-IP approach, the miniTurbo-based method using an intracellular biotin ligase tag could not capture extracellular interactors of MpSYP12A and MpSYP13B, which can be a drawback for certain applications. Extracellular proteins can be captured by tagging biotin ligases to extracellular regions of bait proteins. However, it remains to be determined whether the miniTurbo-based approach is also suitable for other cellular compartments and extracellular space, which may have a different pH or temperature, as discussed by Mair & Bergmann (2021).

To date, a manifold of interaction partners of AtSYP1 family proteins have been identified or predicted (Kwon *et al.*, 2008; *Arabidopsis* Interactome Mapping Consortium, 2011; Fujiwara *et al.*, 2014). With our miniTurbo-based approach, we were able to capture homologues to well-known AtSYP1-interacting proteins, such as KEU, NPSN11, SYP61 and VAMP721 (Fujiwara *et al.*, 2014), demonstrating the reliability of our method. We identified 47 and 40 proteins that are homologous to previously described AtSYP1-interacting proteins, while 104 and 92 proteins were linked to 'vesicle-mediated transport' based on our GO term enrichment analysis. This indicates that we were able to capture a number of undescribed potential interactors of MpSYP12A and MpSYP13B, respectively. Kanazawa *et al.* (2020) showed that MpSYP12A but not MpSYP13B localized to the phragmoplast during cell plate formation by using fluorescent reporter lines. Based on our GO term enrichment analysis, we found the same set of 30 proteins related to 'cell plate formation' in interactomes of both MpSYP12A and MpSYP13B. In other words, we failed to identify unique potential interactors of MpSYP12A previously linked to 'cell plate formation'. To address a role of MpSYP12A at the phragmoplast, experimental conditions would need to be further adjusted to capture the interactome during cell division, by using cell cycle-specific promoters to express proteins in dividing cells, for instance.

Our miniTurbo-based approach identified a number of potential interactors that are specific for MpSYP12A and MpSYP13B, which may help to understand functional differences between the two SNAREs in the future. For example, we found that homologues to MILDEW RESISTANCE LOCUS O (MLO) and PENETRATION 3 (PEN3) preferentially interact with MpSYP12A. *MLO* genes were shown to be involved in susceptibility to powdery mildew pathogens in barley (Büschges *et al.*, 1997) and *A. thaliana* (Consonni *et al.*, 2006). At*PEN3* was found to be involved in resistance against barley powdery mildew (Stein *et al.*, 2006) and cell-death responses upon infection with *Phytopthora infestans* (Kobae *et al.*, 2006). In *A. thaliana*, AtSYP121 or PENETRATION1 (PEN1) is homologous to MpSYP12A. At*PEN1* was shown to be required for SNARE-dependent penetration resistance against barley powdery mildew, and pathogen-induced vesicle accumulation was enhanced in *MLO* loss-of-function mutants (Collins *et al.*, 2003). Recently,

Table 1 Potential interactors that preferentially interact with MpSYP12A or MpSYP13B.

No.	MpGene ID	*A. thaliana* homologue (AGI code)	Annotation	Log$_2$ fold-change MpSYP13B/MpSYP12A	−log *P*-value	Exclusive
1	Mp1g19980	–	LAMA3	−5.05	4.41	No
2	Mp2g10520	AT4G31080	Membrane protein	−4.69	3.34	MpSYP12A
3	Mp3g21160	AT1G67230	MpNMCP	−3.92	3.16	MpSYP12A
4	Mp3g05990	AT3G10650	NUP57	−3.52	3.32	No
5	Mp1g10960	–	Mp1g10960	−3.48	1.52	No
6	Mp1g28560	AT1G47750	PEX11	−3.37	3.21	No
7	Mp6g02820	AT3G47700	RINT1	−3.36	6.14	No
8	Mp3g12450	AT4G30190	MpHA20	−3.33	1.21	MpSYP12A
9	Mp2g17240	AT5G01950	LRR-kinase	−3.18	2.04	MpSYP12A
10	Mp6g00050	AT1G61290	MpSYP12A	−3.14	2.74	No
11	Mp3g18380	AT1G28490	MpSYP6A	−3.08	1.65	No
12	Mp1g08670	AT1G73200	TEX2	−3.01	2.70	No
13	Mp6g00330	AT4G04910	NSF	−2.81	2.25	No
14	Mp2g14450	AT5G45420	MpMYB3	−2.77	2.31	No
15	Mp7g04560	AT3G55420	AT3G55420-like	−2.74	2.68	No
16	Mp2g20600	AT5G43360	PHO84	−2.70	2.86	No
17	Mp1g14480	AT5G45160	RDH3/SEY1	−2.70	2.98	No
18	Mp3g07700	AT5G62670	MpHA11	−2.69	2.84	No
19	Mp7g14000	AT3G52190	PREB	−2.54	1.41	MpSYP12A
20	Mp7g10500	AT1G20970	AT1G20970-like	−2.53	1.34	No
21	Mp1g28850	AT5G64930	MpCPR	−2.48	1.82	MpSYP12A
22	Mp7g07570	AT1G48090	VPS-associated	−2.45	3.35	No
23	Mp2g19670	AT1G21790	TLC lipid-sens.	−2.42	1.94	No
24	Mp3g14570	AT1G73020	ANO10	−2.31	1.65	No
25	Mp1g21390	AT3G18610	NSR1	−2.28	3.06	No
26	Mp5g01540	AT5G53760	MLO	−2.25	2.83	No
27	Mp3g11440	AT1G48090	VPS-associated	−2.20	1.87	MpSYP12A
28	Mp3g23010	AT2G46225	ABIL1	−2.19	1.01	MpSYP12A
29	Mp2g00370	AT3G05060	NOP58	−2.00	1.36	MpSYP12A
30	Mp1g11950	AT3G16310	NUP35/53	−1.99	1.40	No
31	Mp7g06360	AT3G11950	TRAF zinc finger	−1.93	1.94	No
32	Mp2g17840	AT3G06510	SFR2	−1.88	1.66	MpSYP12A
33	Mp3g16790	AT5G19760	SLC25A11	−1.85	3.86	MpSYP12A
34	Mp4g16700	AT1G30690	SEC14-related	−1.85	3.32	No
35	Mp2g02640	AT1G01230	ORM	−1.80	2.29	MpSYP12A
36	Mp2g10340	AT3G12490	CYSB-like	−1.76	1.75	No
37	Mp4g12650	AT3G57150	MpCBF5	−1.69	1.68	MpSYP12A
38	Mp6g17400	AT3G20500	APC7	−1.67	2.21	No
39	Mp6g16270	AT2G45540	BEACH	−1.65	1.82	No
40	Mp8g00690	AT5G21990	FKBP-TRP	−1.65	5.37	No
41	Mp3g00870	AT5G13560	Citron	−1.64	4.26	No
42	Mp4g16720	AT1G30690	SEC14-related	−1.63	2.30	No
43	Mp5g13890	AT2G39280	Ypt-activating	−1.49	2.07	No
44	Mp8g06300	AT5G01180	PTR5	−1.48	2.88	No
45	Mp8g18220	AT3G60860	BIG	−1.47	2.38	No
46	Mp4g23500	AT1G59820	DRS2	−1.46	2.26	No
47	Mp3g01730	AT1G28250	AT1G28250-like	−1.43	2.25	No
48	Mp1g04630	AT5G44240	ALA2	−1.40	4.95	No
49	Mp6g07760	AT1G12360	KEU	−1.37	2.90	No
50	Mp5g23560	AT3G62860	Lysophospholipase	−1.33	2.77	No
51	Mp2g00520	–	Mp2g00520	−1.19	4.22	No
52	Mp4g07450	AT3G28860	MpABCB5	−1.02	2.84	No
53	Mp6g13120	AT5G14240	Phosducin-like	1.07	3.14	No
54	Mp3g04380	AT3G09030	EAP3	1.17	2.74	No
55	Mp2g17470	AT1G68410	PP2C	1.40	2.68	No
56	Mp2g15040	AT4G01070	UGT72E	1.70	1.89	No
57	Mp5g04500	AT3G04810	MpNEK	1.73	2.42	MpSYP13B
58	Mp6g00440	AT1G22610	Synaptogamin-like	2.21	1.72	No
59	Mp7g09750	AT2G41740	VLN2	2.25	2.61	No
60	Mp3g14990	AT4G14605	mTERF	3.17	0.94	No
61	Mp2g19600	AT3G03800	MpSYP13B	6.69	4.11	No

Proteins that are highlighted in turquoise or magenta in Fig. 4 are listed.

Rubiato *et al.* (2021) provided evidence for an evolutionarily conserved role of SYP12 proteins in the formation of papillae and encasements at pathogen penetration sites, which are effective defence structures against a broad range of filamentous pathogens. Together, our data suggest a function of MpSYP12A in penetration resistance and responses to filamentous pathogens, such as SYP12 proteins in other plant species. In addition, we found that MpSYP12A may exclusively interact with ABSCISIC ACID INSENSITIVE1 (MpABI1), NUCLEAR MATRIX CONSTITUENT PROTEIN (MpNMCP), and homologues of OROSOMUCOID-LIKE 1 (ORM1) and SENSITIVE TO FREEZING 2 (SFR2). MpABI1 is involved in abscisic acid signalling (Tougane *et al.*, 2010) and MpNMCP was found to function in stress signalling in *M. polymorpha* (Wang *et al.*, 2021). In *A. thaliana*, NMCP homologues play a role in immunity (Choi *et al.*, 2019; Jarad *et al.*, 2019). AtORMs were reported to play roles in sphingolipid homeostasis and stress responses (Li *et al.*, 2016), and AtSFR2 is a membrane remodelling enzyme responsive to freezing conditions in *A. thaliana* (Barnes *et al.*, 2019). Accordingly, our findings suggest a potential role of MpSYP12A in lipid homeostasis and stress responses. We identified MpNEK1 as a potential exclusive interactor for MpSYP13B. MpNEK1 directs tip growth in rhizoids of *M. polymorpha* (Otani *et al.*, 2018), and thus our data suggest a potential role of MpSYP13B in rhizoid tip growth. Note that potential interactors revealed by PL need to be validated using complementary approaches. In summary, our interactome data should be a useful resource for future investigations of functional conservation and diversification of SNARE proteins in plants.

Author contributions

KM and HN designed the research. KM, SCS, AH and HN contributed to experimental design and workflow conceptualization. KM, SCS and AH conducted experiments. KM, SCS and HN analysed the data by mass spectrometry. KM, SCS and HN wrote the manuscript.

ORCID

Anne Harzen (ID) https://orcid.org/0000-0001-7370-4939
Katharina Melkonian (ID) https://orcid.org/0000-0001-7627-0953
Hirofumi Nakagami (ID) https://orcid.org/0000-0003-2569-7062
Sara Christina Stolze (ID) https://orcid.org/0000-0002-1421-9703

Data availability

The MS proteomics data have been deposited in the ProteomeXchange Consortium via the PRIDE partner repository with the dataset identifier PXD030429.

References

Arabidopsis Interactome Mapping Consortium. 2011. Evidence for network evolution in an *Arabidopsis* interactome map. *Science* **333**: 601–607.

Arora D, Abel NB, Liu C, Van Damme P, Yperman K, Eeckhout D, Vu LD, Wang J, Tornkvist A, Impens F *et al.* 2020. Establishment of proximity-dependent biotinylation approaches in different plant model systems. *Plant Cell* **32**: 3388–3407.

Baldet P, Alban C, Douce R. 1997. Biotin synthesis in higher plants: purification and characterization of *bioB* gene product equivalent from *Arabidopsis thaliana* overexpressed in *Escherichia coli* and its subcellular localization in pea leaf cells. *FEBS Letters* **419**: 206–210.

Baldet P, Gerbling H, Axiotis S, Douce R. 1993. Biotin biosynthesis in higher plant cells. *European Journal of Biochemistry* **217**: 479–485.

Barnes AC, Elowsky CG, Roston RL. 2019. An Arabidopsis protoplast isolation method reduces cytosolic acidification and activation of the chloroplast stress sensor SENSITIVE TO FREEZING 2. *Plant Signaling & Behavior* **14**: 1629270.

Batoko H, Moore I. 2001. Plant cytokinesis: Knolle joins the club. *Current Biology* **11**: R423–R426.

Bowman JL, Kohchi T, Yamato KT, Jenkins J, Shu S, Ishizaki K, Yamaoka S, Nishihama R, Nakamura Y, Berger F *et al.* 2017. Insights into land plant evolution garnered from the *Marchantia polymorpha* genome. *Cell* **171**: 287–304.e15.

Branon TC, Bosch JA, Sanchez AD, Udeshi ND, Svinkina T, Carr SA, Feldman JL, Perrimon N, Ting AY. 2018. Efficient proximity labeling in living cells and organisms with TurboID. *Nature Biotechnology* **36**: 880–887.

Büschges R, Hollricher K, Panstruga R, Simons G, Wolter M, Frijters A, van Daelen R, van der Lee T, Diergaarde P, Groenendijk J *et al.* 1997. The barley *Mlo* gene: a novel control element of plant pathogen resistance. *Cell* **88**: 695–705.

Carella P, Gogleva A, Tomaselli M, Alfs C, Schornack S. 2018. *Phytophthora palmivora* establishes tissue-specific intracellular infection structures in the earliest divergent land plant lineage. *Proceedings of the National Academy of Sciences, USA* **115**: E3846–E3855.

Catalano CM, Czymmek KJ, Gann JG, Sherrier DJ. 2007. *Medicago truncatula* syntaxin SYP132 defines the symbiosome membrane and infection droplet membrane in root nodules. *Planta* **225**: 541–550.

Chawade A, Alexandersson E, Levander F. 2014. NORMALYZER: a tool for rapid evaluation of normalization methods for omics data sets. *Journal of Proteome Research* **13**: 3114–3120.

Choi J, Strickler SR, Richards EJ. 2019. Loss of CRWN nuclear proteins induces cell death and salicylic acid defense signaling. *Plant Physiology* **179**: 1315–1329.

Collins NC, Thordal-Christensen H, Lipka V, Bau S, Kombrink E, Qiu J-L, Hückelhoven R, Stein M, Freialdenhoven A, Somerville SC *et al.* 2003. SNARE-protein-mediated disease resistance at the plant cell wall. *Nature* **425**: 973–977.

Consonni C, Humphry ME, Hartmann HA, Livaja M, Durner J, Westphal L, Vogel J, Lipka V, Kemmerling B, Schulze-Lefert P *et al.* 2006. Conserved requirement for a plant host cell protein in powdery mildew pathogenesis. *Nature Genetics* **38**: 716–720.

Cox J, Mann M. 2008. MAXQUANT enables high peptide identification rates, individualized p.p.b.-range mass accuracies and proteome-wide protein quantification. *Nature Biotechnology* **26**: 1367–1372.

Enami K, Ichikawa M, Uemura T, Kutsuna N, Hasezawa S, Nakagawa T, Nakano A, Sato MH. 2009. Differential expression control and polarized

distribution of plasma membrane-resident SYP1 SNAREs in *Arabidopsis thaliana*. *Plant and Cell Physiology* 50: 280–289.

Fujiwara M, Uemura T, Ebine K, Nishimori Y, Ueda T, Nakano A, Sato MH, Fukao Y. 2014. Interactomics of Qa-SNARE in *Arabidopsis thaliana*. *Plant and Cell Physiology* 55: 781–789.

Hirano T, Ebine K, Ueda T, Higaki T, Nakayama T, Konno H, Takigawa-Imamura H, Sato MH. 2020. The SYP123-VAMP727 SNARE complex is involved in the delivery of inner cell wall components to the root hair shank in Arabidopsis. *bioRxiv*. doi: 10.1101/2020.12.28.424500.

Ichikawa M, Hirano T, Enami K, Fuselier T, Kato N, Kwon C, Voigt B, Schulze-Lefert P, Baluska F, Sato MH. 2014. Syntaxin of plant proteins SYP123 and SYP132 mediate root hair tip growth in *Arabidopsis thaliana*. *Plant and Cell Physiology* 55: 790–800.

Ishizaki K, Chiyoda S, Yamato KT, Kohchi T. 2008. *Agrobacterium*-mediated transformation of the haploid liverwort *Marchantia polymorpha* L., an emerging model for plant biology. *Plant and Cell Physiology* 49: 1084–1091.

Ishizaki K, Johzuka-Hisatomi Y, Ishida S, Iida S, Kohchi T. 2013. Homologous recombination-mediated gene targeting in the liverwort *Marchantia polymorpha* L. *Scientific Reports* 3: 1532.

Ishizaki K, Nishihama R, Ueda M, Inoue K, Ishida S, Nishimura Y, Shikanai T, Kohchi T. 2015. Development of gateway binary vector series with four different selection markers for the liverwort *Marchantia polymorpha*. *PLoS ONE* 10: e0138876.

Jarad M, Mariappan K, Almeida-Trapp M, Mette MF, Mithofer A, Rayapuram N, Hirt H. 2019. The Lamin-like LITTLE NUCLEI 1 (LINC1) regulates pattern-triggered immunity and jasmonic acid signaling. *Frontiers in Plant Science* 10: 1639.

Johansson ON, Fantozzi E, Fahlberg P, Nilsson AK, Buhot N, Tor M, Andersson MX. 2014. Role of the penetration-resistance genes *PEN1*, *PEN2* and *PEN3* in the hypersensitive response and race-specific resistance in *Arabidopsis thaliana*. *The Plant Journal* 79: 466–476.

Kanazawa T, Era A, Minamino N, Shikano Y, Fujimoto M, Uemura T, Nishihama R, Yamato KT, Ishizaki K, Nishiyama T et al. 2016. SNARE molecules in *Marchantia polymorpha*: unique and conserved features of the membrane fusion machinery. *Plant and Cell Physiology* 57: 307–324.

Kanazawa T, Morinaka H, Ebine K, Shimada TL, Ishida S, Minamino N, Yamaguchi K, Shigenobu S, Kohchi T, Nakano A et al. 2020. The liverwort oil body is formed by redirection of the secretory pathway. *Nature Communications* 11: 6152.

Kobae Y, Sekino T, Yoshioka H, Nakagawa T, Martinoia E, Maeshima M. 2006. Loss of AtPDR8, a plasma membrane ABC transporter of *Arabidopsis thaliana*, causes hypersensitive cell death upon pathogen infection. *Plant and Cell Physiology* 47: 309–318.

Kubota A, Ishizaki K, Hosaka M, Kohchi T. 2013. Efficient *Agrobacterium*-mediated transformation of the liverwort *Marchantia polymorpha* using regenerating thalli. *Bioscience, Biotechnology, and Biochemistry* 77: 167–172.

Kwon C, Neu C, Pajonk S, Yun HS, Lipka U, Humphry M, Bau S, Straus M, Kwaaitaal M, Rampelt H et al. 2008. Co-option of a default secretory pathway for plant immune responses. *Nature* 451: 835–840.

Lamesch P, Berardini TZ, Li D, Swarbreck D, Wilks C, Sasidharan R, Muller R, Dreher K, Alexander DL, Garcia-Hernandez M et al. 2012. The Arabidopsis Information Resource (TAIR): improved gene annotation and new tools. *Nucleic Acids Research* 40: D1202–D1210.

Li J, Yin J, Rong C, Li KE, Wu JX, Huang LQ, Zeng HY, Sahu SK, Yao N. 2016. Orosomucoid proteins interact with the small subunit of serine Palmitoyltransferase and contribute to sphingolipid homeostasis and stress responses in Arabidopsis. *Plant Cell* 28: 3038–3051.

Ludwig A, Stolz J, Sauer N. 2000. Plant sucrose-H+ symporters mediate the transport of vitamin H. *The Plant Journal* 24: 503–509.

Mair A, Bergmann DC. 2021. Advances in enzyme-mediated proximity labeling and its potential for plant research. *Plant Physiology* 188: 756–768.

Mair A, Xu SL, Branon TC, Ting AY, Bergmann DC. 2019. Proximity labeling of protein complexes and cell-type-specific organellar proteomes in *Arabidopsis* enabled by TurboID. *eLife* 8: e47864.

von Mering C, Huynen M, Jaeggi D, Schmidt S, Bork P, Snel B. 2003. STRING: a database of predicted functional associations between proteins. *Nucleic Acids Research* 31: 258–261.

Mi H, Ebert D, Muruganujan A, Mills C, Albou LP, Mushayamaha T, Thomas PD. 2021. PANTHER v.16: a revised family classification, tree-based classification tool, enhancer regions and extensive API. *Nucleic Acids Research* 49: D394–D403.

Montgomery SA, Tanizawa Y, Galik B, Wang N, Ito T, Mochizuki T, Akimcheva S, Bowman JL, Cognat V, Maréchal-Drouard L et al. 2020. Chromatin organization in early land plants reveals an ancestral association between H3K27me3, transposons, and constitutive heterochromatin. *Current Biology* 30: 573–588.e7.

Orchard S, Ammari M, Aranda B, Breuza L, Briganti L, Broackes-Carter F, Campbell NH, Chavali G, Chen C, del-Toro N et al. 2014. The MIntAct project–IntAct as a common curation platform for 11 molecular interaction databases. *Nucleic Acids Research* 42: D358–D363.

Otani K, Ishizaki K, Nishihama R, Takatani S, Kohchi T, Takahashi T, Motose H. 2018. An evolutionarily conserved NIMA-related kinase directs rhizoid tip growth in the basal land plant *Marchantia polymorpha*. *Development* 145: dev154617.

Pommerrenig B, Popko J, Heilmann M, Schulmeister S, Dietel K, Schmitt B, Stadler R, Feussner I, Sauer N. 2013. SUCROSE TRANSPORTER 5 supplies Arabidopsis embryos with biotin and affects triacylglycerol accumulation. *The Plant Journal* 73: 392–404.

Rappsilber J, Ishihama Y, Mann M. 2003. Stop and go extraction tips for matrix-assisted laser desorption/ionization, nanoelectrospray, and LC/MS sample pretreatment in proteomics. *Analytical Chemistry* 75: 663–670.

Reichardt I, Slane D, El Kasmi F, Knoll C, Fuchs R, Mayer U, Lipka V, Jurgens G. 2011. Mechanisms of functional specificity among plasma-membrane syntaxins in *Arabidopsis*. *Traffic* 12: 1269–1280.

Rubiato HM, Liu M, O'Connell RJ, Nielsen ME. 2021. Plant SYP12 syntaxins mediate an evolutionarily conserved general immunity to filamentous pathogens. *bioRxiv*. doi: 10.1101/2020.02.21.957480.

Saito S, Hirao Y, Quadery AF, Xu B, Elguoshy A, Fujinaka H, Koma S, Yamamoto K, Yamamoto T. 2019. The optimized workflow for sample preparation in LC-MS/MS-based urine proteomics. *Methods and Protocols* 2: 46.

Sanderfoot A. 2007. Increases in the number of SNARE genes parallels the rise of multicellularity among the green plants. *Plant Physiology* 144: 6–17.

Silva PA, Ul-Rehman R, Rato C, Di Sansebastiano G-P, Malhó R. 2010. Asymmetric localization of *Arabidopsis* SYP124 syntaxin at the pollen tube apical and sub-apical zones is involved in tip growth. *BMC Plant Biology* 10: 1–12.

Stark C, Breitkreutz BJ, Reguly T, Boucher L, Breitkreutz A, Tyers M. 2006. BIOGRID: a general repository for interaction datasets. *Nucleic Acids Research* 34: D535–D539.

Stein M, Dittgen J, Sanchez-Rodriguez C, Hou BH, Molina A, Schulze-Lefert P, Lipka V, Somerville S. 2006. *Arabidopsis* PEN3/PDR8, an ATP binding cassette transporter, contributes to nonhost resistance to inappropriate pathogens that enter by direct penetration. *Plant Cell* 18: 731–746.

Sun Q, Zybailov B, Majeran W, Friso G, Olinares PD, vanWijk KJ. 2009. PPDB, the plant proteomics database at Cornell. *Nucleic Acids Research* 37: D969–D974.

Tougane K, Komatsu K, Bhyan SB, Sakata Y, Ishizaki K, Yamato KT, Kohchi T, Takezawa D. 2010. Evolutionarily conserved regulatory mechanisms of abscisic acid signaling in land plants: characterization of *ABSCISIC ACID INSENSITIVE1-like* type 2C protein phosphatase in the liverwort *Marchantia polymorpha*. *Plant Physiology* 152: 1529–1543.

Tyanova S, Temu T, Cox J. 2016. The MAXQUANT computational platform for mass spectrometry-based shotgun proteomics. *Nature Protocols* 11: 2301–2319.

Uemura T, Kim H, Saito C, Ebine K, Ueda T, Schulze-Lefert P, Nakano A. 2012. Qa-SNAREs localized to the *trans*-Golgi network regulate multiple transport pathways and extracellular disease resistance in plants. *Proceedings of the National Academy of Sciences, USA* 109: 1784–1789.

Uemura T, Ueda T, Ohniwa RL, Nakano A, Takeyasu K, Sato MH. 2004. Systematic analysis of SNARE molecules in *Arabidopsis*: dissection of the post-Golgi Network in plant cells. *Cell Structure and Function* 29: 49–65.

Wang N, Karaaslan ES, Faiss N, Berendzen KW, Liu C. 2021. Characterization of a plant nuclear matrix constituent protein in liverwort. *Frontiers in Plant Science* 12: 670306.

Wisniewski JR, Zougman A, Nagaraj N, Mann M. 2009. Universal sample preparation method for proteome analysis. *Nature Methods* 6: 359–362.

Xia L, Mar Marques-Bueno M, Bruce CG, Karnik R. 2019. Unusual roles of secretory SNARE SYP132 in plasma membrane H(+)-ATPase traffic and vegetative plant growth. *Plant Physiology* **180**: 837–858.

Yun HS, Kang BG, Kwon C. 2016. Arabidopsis immune secretory pathways to powdery mildew fungi. *Plant Signaling & Behavior* **11**: e1226456.

Zhang Y, Li Y, Wen Z, Nagalakshmi U, Dinesh-Kumar SP. 2021. TurboID-based proximity labeling for in planta identification of protein-protein interaction networks. *Journal of Visualized Experiments* **159**. doi: 10.3791/60728.

Zhang Y, Song G, Lal NK, Nagalakshmi U, Li Y, Zheng W, Huang P-J, Branon TC, Ting AY, Walley JW et al. 2019. TurboID-based proximity labeling reveals that UBR7 is a regulator of N NLR immune receptor-mediated immunity. *Nature Communications* **10**: 3252.

Zhou Y, Zhou B, Pache L, Chang M, Khodabakhshi AH, Tanaseichuk O, Benner C, Chanda SK. 2019. Metascape provides a biologist-oriented resource for the analysis of systems-level datasets. *Nature Communications* **10**: 1523.

Supporting Information

Additional Supporting Information may be found online in the Supporting Information section at the end of the article.

Dataset S1 MpSYP interactome data.

Dataset S2 Reported and predicted interactors of AtSYP1 proteins.

Dataset S3 Homologues of the AtSYP1 interactors in *Marchantia polymorpha.*

Dataset S4 Gene ontology (GO) term enrichment analysis of the MpSYP interactomes.

Fig. S1 Nucleotide and amino acid sequence of the miniTurbo biotin ligase used in this study.

Fig. S2 Plasmid maps of the binary vectors, pMKMM23 and pMKMM22, used in this study.

Fig. S3 Evaluation of the fusion protein expression, biotin depletion methods, and Myc-Trap coimmunoprecipitation (Co-IP) by immunoblotting.

Fig. S4 Biotin ligase activity in *Marchantia polymorpha.*

Fig. S5 Gene ontology (GO) term enrichment analysis of 4 h proximity-dependent *in vivo* labelling (PL) samples.

Fig. S6 Uncropped images of immunoblots used in the figures.

Please note: Wiley Blackwell are not responsible for the content or functionality of any Supporting Information supplied by the authors. Any queries (other than missing material) should be directed to the *New Phytologist* Central Office.